LA-9754-MS

Los Alamos National Laboratory is operated by the University of California for the United States Department of Energy under contract W-7405-ENG-36.

Magnetic Analysis of the Fusion Engineering Device Conceptual Inboard Configuration

Los Alamos Los Alamos National Laboratory
Los Alamos, New Mexico 87545

This work was supported by the US Department of Energy, Office of Fusion Energy.

LA-9754-MS

UC-20d
Issued: April 1983

Nucleonic Analysis of the Fusion Engineering Device Conceptual Inboard Configuration

W. T. Urban

Los Alamos National Laboratory
Los Alamos, New Mexico 87545

CONTENTS

NUCLEONIC ANALYSIS OF THE FUSION ENGINEERING DEVICE CONCEPTUAL INBOARD CONFIGURATION

by

W. T. Urban

ABSTRACT

Three different nucleonic analyses of the Fusion Engineering Device inboard-shield/toroidal-field coil magnet configuration have been performed using the one- and two-dimensional discrete-ordinates codes ONEDANT and TRIDENT-CTR. The three calculational models considered were a one-dimensional cylindrical geometry model with a spatially uniform source, a two-dimensional (r,z) model with a spatially uniform source, and the same two-dimensional model but with a spatially dependent source which is representative of the expected spatial generation of 14-MeV neutrons in a poloidal cross section through the plasma. Each of the calculational models extended inboard to include both the inboard shield and the toroidal-field coil magnet and also to include enough of the outboard shield to obtain a realistic representation of the albedo from that shield. Results of these calculations are intercompared and are used to evaluate the inboard-shield design through a comparison with design criteria for the inboard toroidal-field coil magnet.

I. INTRODUCTION

Prior to the neutronics analysis of a fusion reactor shield, the designer must decide on the spatial dimensionality of the model and the source representation to be used in the calculations. As approximations to the geometry and the source are usually required, the question arises regarding the accuracy of the solution obtained. This report provides some insight to these problems for the Fusion Engineering Device (FED) through a presentation of three different neutronics analyses of the FED inboard configuration. Furthermore, results from these analyses are intercompared and discussed relative to the design criteria for the inboard toroidal-field (TF) coil magnet.

The three calculational models considered were a one-dimensional cylindrical geometry model with a spatially uniform source, a two-dimensional (r,z) model with a spatially uniform source, and the same two-dimensional model but with a spatially dependent source that is representative of the expected spatial distribution at which 14-MeV neutrons are produced in a poloidal cross section of the plasma. Each of the geometry models extended inboard to include the inboard shield and TF coil magnet and also included enough of the outboard shield to obtain a realistic albedo from that shield. These calculations were performed with the one- and two-dimensional discrete-ordinates codes ONEDANT[1] and TRIDENT-CTR,[2] respectively.

The accuracy of a FED inboard-shield evaluation is directly dependent on how well the energy and angular distributions of neutrons and gamma rays incident on the shield are determined in the calculation. This requirement indicates a primary shortcoming of a one-dimensional calculation; i.e., the scattered component of the radiation as well as the source energy radiation incident on the inboard shield is in error because of modeling restraints in the geometry and source representation. For this reason less space is devoted to the one-dimensional calculational results. However, enough are presented to allow comparisons with the two-dimensional results. Because of the unique modeling capabilities of TRIDENT-CTR and the symmetry of the FED about its toroidal axis, an accurate representation of the plasma chamber and the surrounding shielding can be achieved, thereby allowing a more accurate determination of the energy and angular distributions of the radiation incident on the inboard shield. The accuracy of the two-dimensional calculations is then more heavily dependent on the source model used in the calculation.

The ONEDANT and TRIDENT-CTR codes used are available to the fusion community through the National Magnetic Fusion Energy Computer Center (NMFECC) and the Radiation Shielding Information Center (RSIC). Similarly, the Monte Carlo code MCNP,[3] which was used in normalizing the discrete-ordinates calculations and verifying the source modeling, as well as the codes for generating cross-section sets for the calculations are available on the NMFECC. Thus, the calculational approach used should be generally available to fusion reactor shield designers, and the results presented in this report should be conveniently reproducible.

An attempt has been made to extract as much useful information from the calculations as possible. Quite often large calculations are performed and only those results that are immediately in demand are extracted from the calculated results. The objective here has been to provide not only the "desired quantities of interest" but also some of the more fundamental data in a form which may have a wide interest for other fusion designers regardless of whether they are directly involved with the FED. Finally, an attempt has been made to make meaningful comparisons between the results from the three different calculations.

Organization of this report is as follows. Section II contains a description of the geometric models and input parameters for each of the three calculations. A discussion of the normalization is contained in Sec. III, followed by a presentation of the results and intercomparisons in Sec. IV. Conclusions are provided in Sec. V.

II. CALCULATIONS

The one- and two-dimensional calculations were performed to obtain the energy and spatially dependent neutron and gamma-ray fluxes throughout the FED inboard shield and associated components. These fluxes provide the basic data from which related quantities such as heating rates, copper dpa, and other parameters of interest can be obtained.

A. Geometry Cross Sections and Compositions

The FED configuration is shown in Fig. 1. Because of symmetry about the torus equatorial midplane, only the top one-half of the torus is shown. Figure 2 is a one-dimensional slice through the model at the torus midplane which provides more detail as to the materials and their thicknesses. The outboard shield, which also includes the shield above and below the plasma region, is shown at less than

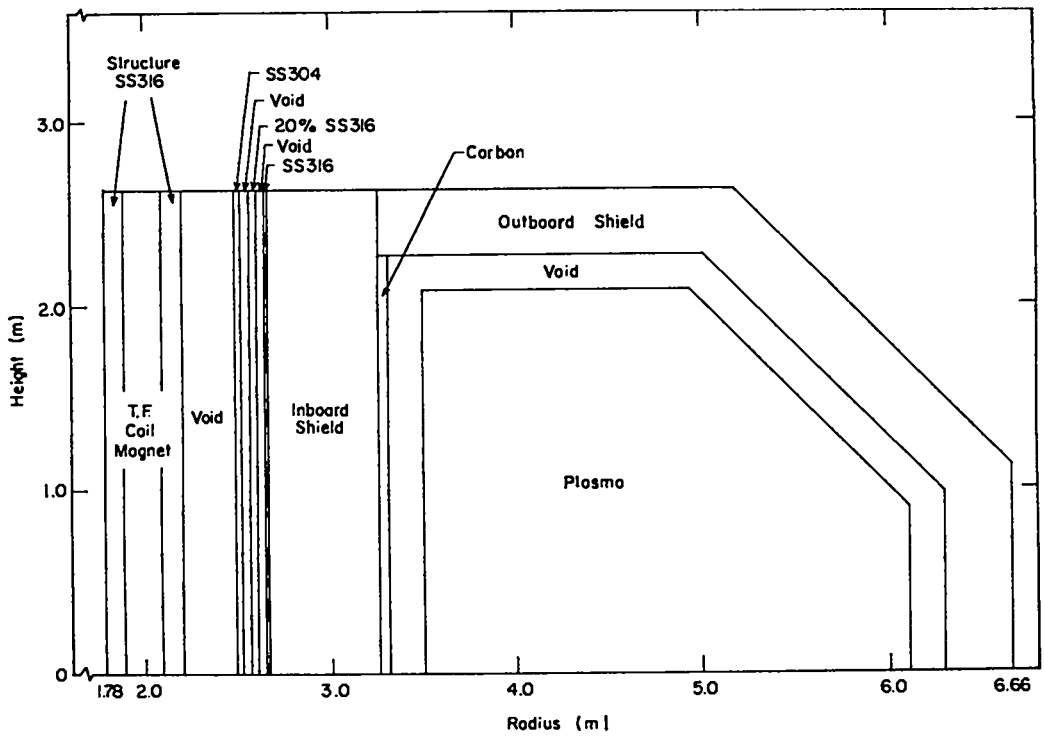

Fig. 1. Conceptual FED configuration.

its design thickness. This reduced thickness approximation is possible because only enough of the outboard shield was required to allow an accurate calculation of the radiation which scatters from it and subsequently is incident on the inboard shield; i.e., it was included only to get an accurate albedo from the outboard shield. This outboard-shield approximation, which used a 0.45-m outboard shield, was verified by one-dimensional calculations.

The nuclear cross sections used were generated from a standard Los Alamos 30/12-group coupled neutron/gamma-ray MATXS[4] library (ENDF/B-V) using the TRANSX[5] and MIXIT codes at the NMFECC. A P_3 scattering approximation was used and the cross sections were transport-corrected using the Bell, Hansen, and Sandmeier methodology.[6] The 30/12-energy-group structure is presented in Table I. Isotopic compositions of the materials indicated in Figs. 1 and 2 are listed in Table II. .

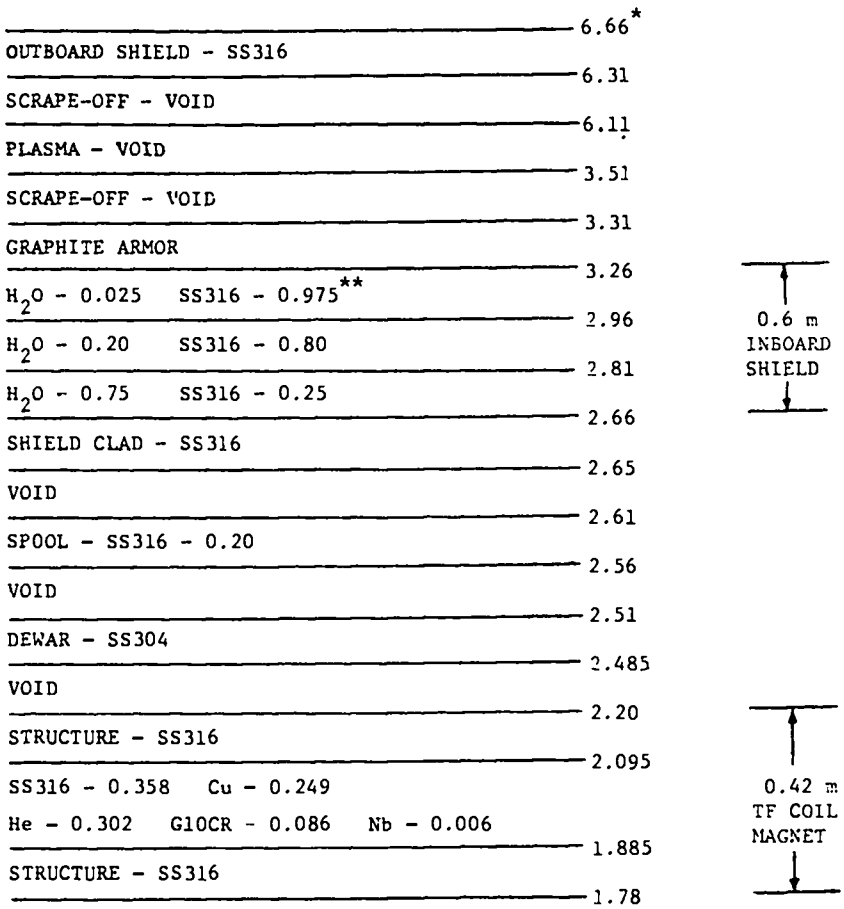

* Radial distance from the torus centerline in meters.

** Volume fraction.

Fig. 2. Radial slice through the FED configuration at the torus equatorial midplane.

B. Two-Dimensional Calculation with Spatially Distributed Source

This two-dimensional calculation, which used a spatially distributed source of 14-MeV neutrons, was performed using the TRIDENT-CTR code. The geometric model was identical to that shown in Fig. 1. In this (r,z) model the z-axis was congruent with the toroidal axis and the r-axis with the torus equatorial midplane.

TABLE I

30/12-ENERGY-GROUP STRUCTURE

E-upper (MeV)	Group	E-Lower (MeV)	E-Upper (MeV)	Group	E-Lower (MeV)
	Neutrons				
1.700+01	1	1.500+01	6.140-05	24	2.260-05
1.500+01	2	1.350+01	2.260-05	25	8.320-06
1.350+01	3	1.200+01	8.320-06	26	3.060-06
1.200+01	4	1.000+01	3.060-06	27	1.130-06
1.000+01	5	7.790+00	1.130-06	28	4.140-07
7.790+00	6	6.070+00	4.140-07	29	1.520-07
6.070+00	7	3.680+00	1.520-07	30	1.390-10
3.680+00	8	2.865+00			
2.865+00	9	2.232+00			
2.232+00	10	1.738+00			
1.738+00	11	1.353+00		Gamma Rays	
1.353+00	12	8.230-01	1.000+01	1	9.000+00
8.230-01	13	5.000-01	9.000+00	2	8.000+00
5.000-01	14	3.030-01	8.000+00	3	7.000+00
3.030-01	15	1.840-01	7.000+00	4	6.000+00
1.840-01	16	6.760-02	6.000+00	5	5.000+00
6.760-02	17	2.480-02	5.000+00	6	4.000+00
2.480-02	18	9.120-03	4.000+00	7	3.000+00
9.120-03	19	3.350-03	3.000+00	8	2.000+00
3.350-03	20	1.235-03	2.000+00	9	1.000+00
1.235-03	21	4.540-04	1.000+00	10	5.000-01
4.540-04	22	1.670-04	5.000-01	11	1.000-01
1.670-04	23	6.140-05	1.000-01	12	1.000-02

TABLE II

ATOM DENSITIES OF MATERIALS

Element	Atoms/m^3
Stainless Steel 316	
Ni	1.15 + 28[a]
Cr	1.67 + 28
Fe	5.44 + 28
Mn	1.75 + 27
Mo	1.51 + 27
Stainless Steel 304	
Ni	7.40 + 27
Cr	1.77 + 28
Fe	6.06 + 28
Mn	1.76 + 27
Water	
H	6.70 + 28
O	3.35 + 28
Carbon	
C	8.03 + 28
Copper	
Cu	8.46 + 28
Liquid Helium	
He	2.21 + 28
Niobium	
Nb	4.07 + 28
G10 CR Insulation	
H	4.41 + 28
^{10}B	3.46 + 26
^{11}B	1.40 + 27
C	2.21 + 28
O	2.52 + 28
Al	2.11 + 27
Si	6.50 + 27
Ca	2.81 + 27

[a] $1.15 + 28 = 1.15 \times 10^{28}$.

Because TRIDENT-CTR uses triangular finite elements, it was possible to accurately model the tapered portions of the outboard shield and thus develop a TRIDENT-CTR model identical to the FED geometry shown in Fig. 1.

The TRIDENT-CTR spatial mesh is shown in Fig. 3. The mesh consisted of 26 bands with the number of triangles per band varying from 67 to 92. The total number of triangles in the model is 2116. Group-dependent quadrature sets were used with an S_8 EQ_N set being the highest order.[7] The selection of quadratures, number of bands, and triangles per band followed that used for the two-dimensional spatially uniform source calculations with the exception that a finer mesh structure was used in the plasma region to allow an accurate representation of the spatial dependence of the source. Boundary conditions used were as follows:

1. A reflective boundary was used along the z-axis at r = 1.78 m (left boundary). This is an approximation predicated on the truncation of the model at this radius. However, it was determined from one-dimensional calculations that this approximation did not influence the results at the radii of interest.
2. A reflective boundary was used along the bottom of the problem domain, which is the torus equatorial midplane and plane of symmetry.
3. Vacuum boundary conditions were used along the right and top surfaces of the problem domain.

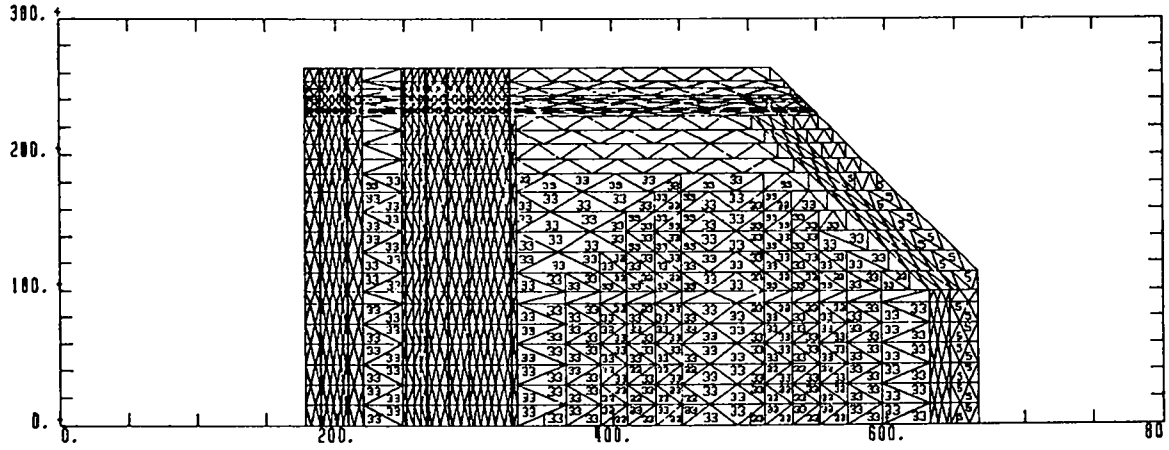

Fig. 3. TRIDENT-CTR mesh for the spatially dependent source case. Dimensions in centimeters.

A spatially dependent source of DT neutrons was used. These 14-MeV neutrons were entered into the calculation by putting the source into energy group 2, i.e., 13.5 to 15.0 MeV. The functional form of this spatially dependent source is

$$F = [1.0 - (\frac{r}{0.88a})^2]^2 \quad , \tag{1}$$

where r = radial distance from the plasma center;

$a = a_o(\cos^2 \theta + b^2 \sin^2 \theta)^{\frac{1}{2}}$;

a_o = plasma minor radius, 1.3 m;

b = aspect ratio, 1.6; and

θ = poloidal angle between the equatorial midplane and r.

Figure 4 illustrates the falloff of the source magnitude as a function of the radial distance from the plasma center. It should be noted that the magnitude of the source varies poloidally as well as radially, but in Fig. 4 the poloidal variation has been suppressed by plotting as a function of (r/0.88a).

Considerable effort was expended to insure that the spatial dependence of the source was introduced into the TRIDENT-CTR calculation in sufficient detail

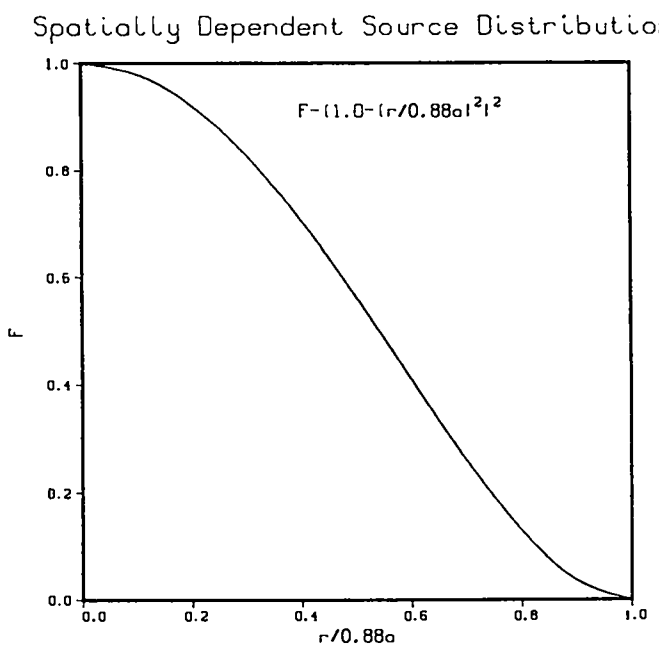

Fig. 4. Spatially dependent source magnitude versus fraction of plasma radius.

to adequately represent the source. The adequacy of the source input was verified through a comparison of the source-energy flux incident on the inboard and outboard shields from TRIDENT-CTR to that from a Monte Carlo calculation performed using MCNP. This was believed to be an adequate test because in MCNP the starting location is obtained by sampling the cumulative distribution function based on the density function of Eq. (1) and is not dependent on any type of mesh structure. Figures 5 and 6 present these comparisons at the outboard and inboard shields, respectively. The fractional error (at the 68% confidence level) of the MCNP results in Fig. 5 is ≤ 0.02 and in Fig. 6 it is <0.04. The agreement between the TRIDENT-CTR and MCNP results is quite good, particularly considering the expanded scale of the ordinate scales, and thus provided a measure of confidence in the way the spatial dependence of the source was introduced into the TRIDENT-CTR calculation.

The TRIDENT-CTR calculation was normalized to one source neutron. The results were subsequently renormalized to reflect a design wall loading of 0.4 MW/m^2 at the outboard shield as described in Sec. III.

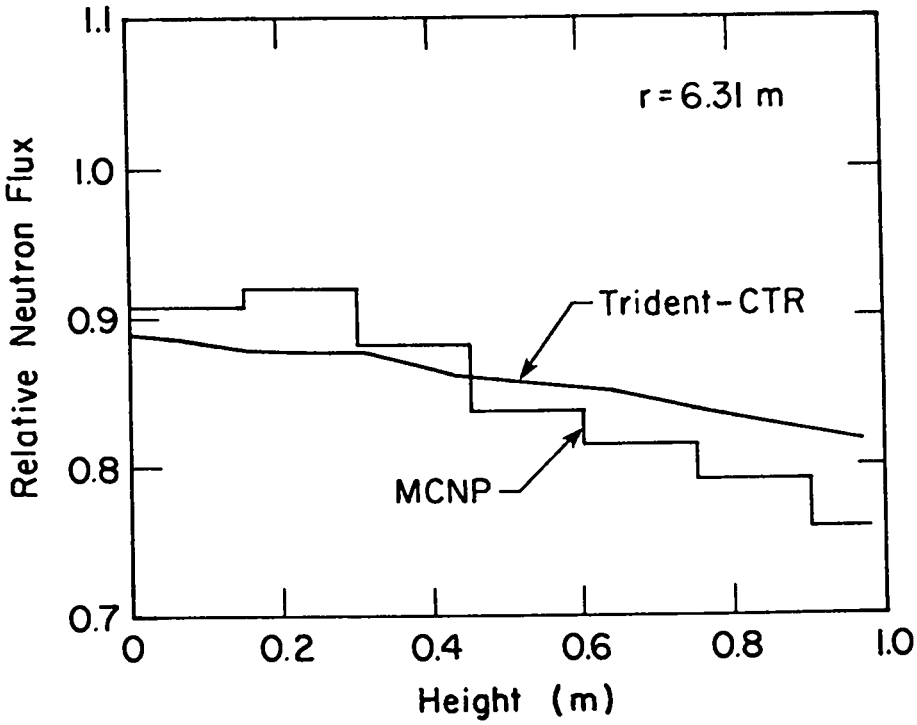

Fig. 5. Comparison of TRIDENT-CTR and MCNP 14-MeV fluxes incident on the outboard shield for the spatially dependent source case.

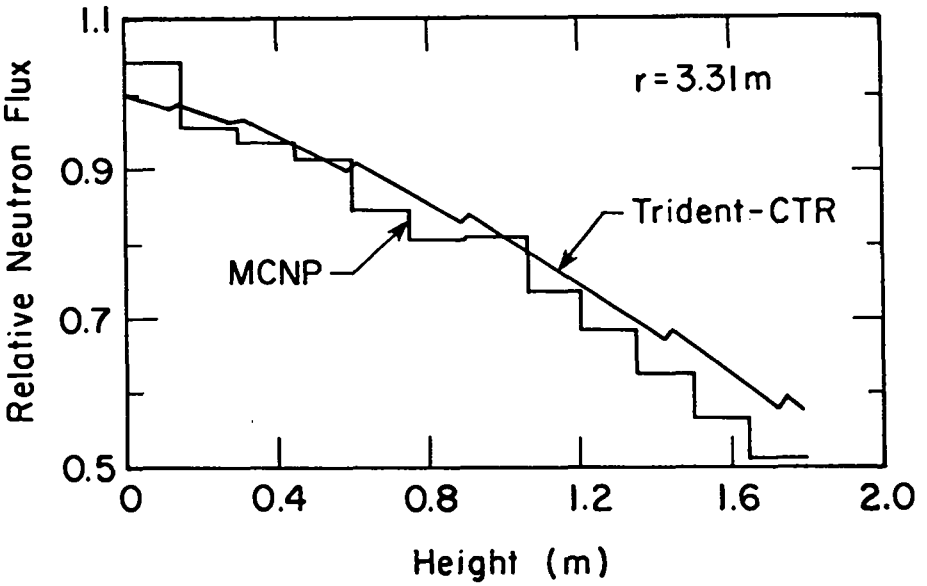

Fig. 6. Comparison of TRIDENT-CTR and MCNP 14-MeV fluxes incident on the inboard shield for the spatially dependent source case.

C. Two-Dimensional Calculation with Spatially Uniform Source

This TRIDENT-CTR calculation was primarily the same as that described above except that in this calculation a spatially uniform source was used. The geometry model used was identical to the model shown in Fig. 1 and was the same as that used in the two-dimensional spatially distributed source calculation except that fewer triangles were used in the plasma region and one more band was used. The spatial mesh used is shown in Fig. 7. The mesh consisted of 27 bands with the number of triangles per band varying from 67 to 83. The total number of triangles in the model was 2062. Again, group-dependent quadrature sets were used with an S_8 EQ_Q set being the highest order. This two-dimensional calculation preceded the one described above and the selection of quadratures, number of bands, and number of triangles per band resulted from parametric studies. However, this does not mean that the mesh is optimized, but rather that it is adequate. Further reduction of the mesh above and to the right of the plasma region could probably be possible without significantly compromising the speed of convergence or the accuracy of the results.

A uniformly distributed source of DT neutrons was used. These 14-MeV neutrons were entered into the calculations by putting the source into energy group 2, i.e., 13.5 to 15.0 MeV. These neutrons were produced with an isotropic angular

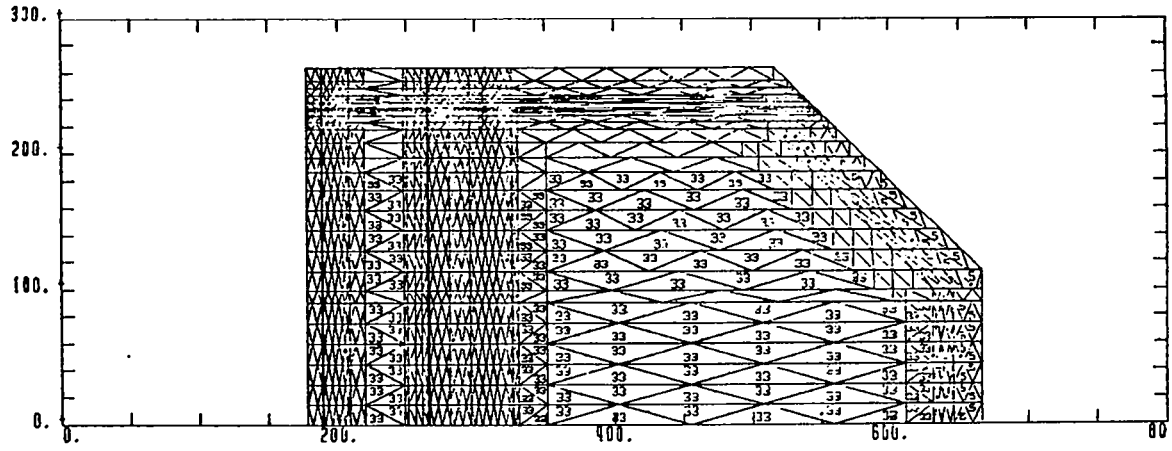

Fig. 7. TRIDENT-CTR mesh for the spatially uniform source case.

distribution. The source volume was 138.6 m^3. The TRIDENT-CTR calculation was normalized to 7.324 x 10^{-3} source neutrons/m^3s, which is numerically equivalent to unity over the source volume. The results were subsequently renormalized to a 0.4-MW/m^2 wall loading at the outboard-shield first wall as discussed in Sec. III.

D. One-Dimensional Calculation with Spatially Uniform Source

The one-dimensional calculation using a spatially uniform source was performed using the ONEDANT code. A cylindrical geometry model based on Fig. 2 was used in this calculation with an outboard-shield thickness of 0.45 m. The calculation was made using an S_8 approximation and a P_3 scattering approximation. The 14-MeV neutron source was uniformly distributed in the radial direction. A reflective boundary condition was used on the left boundary, and a vacuum boundary condition was used on the right boundary.

III. NORMALIZATION

Both the TRIDENT-CTR and the ONEDANT calculations were performed with a normalization to one source neutron. The FED conceptual design specifies a wall loading due to 14-MeV neutrons of 0.4 MW/m^2 at the first wall of the outboard shield. Thus, both the one- and two-dimensional calculational results required renormalization. Because wall loading is based on the outboard directed current

of source-energy neutrons at the outboard-shield first wall, a quantity not directly obtained from the TRIDENT-CTR calculations, the renormalization factors for both the TRIDENT-CTR results were derived from calculations performed using the Monte Carlo code MCNP. This factor relates the outward directed source-energy neutron flow (current) to the source-energy neutron flux at the outboard-shield first wall.

The relationship between the current and the flux of source-energy neutrons at the outboard-shield first wall is a function of the source geometry and its spatial distribution. Therefore, separate Monte Carlo calculations were made to correspond to each of the discrete-ordinate models. Since it is source-energy quantities which are of interest, there is no need to track the particles after they cross into the shield (either inboard or outboard). Thus, the particle histories were terminated when they crossed into the shield regions. This is an approximation in that there is a possibility of neutrons making grazing penetrations of the inboard shield with no energy loss (no interaction). However, the potential of this effect having an impact is very small, particularly given that the angular distribution of neutrons incident on the inboard shield is not tilted toward grazing angles of incidence.

The source representations for these three MCNP models were identical to those used in the corresponding discrete-ordinates models except that for the spatially distributed source the Monte Carlo procedure sampled the discretized cumulative distribution function derived from the source density function of Eq. (1). As discussed earlier, this is a more accurate representation of the source as compared to the mesh approach used with TRIDENT-CTR, provided that the source in adequately sampled. However, in the previous discussion of Figs. 5 and 6 it was demonstrated that both source models yield results which were in agreement at the plasma chamber/shield interface.

Monte Carlo calculations were made with MCNP for each of the models, and the results obtained were used in conjunction with the corresponding discrete-ordinates flux to compute normalization factors. The precise method used for the TRIDENT-CTR normalizations were

$$NF = K \frac{\phi^{MCNP}}{C_{MCNP}} \frac{1}{\phi^{TRD}} \quad , \tag{2}$$

where K = conversion factor (current of 14-MeV neutrons/cm^2s)/(0.4 MW/m^2),

ϕ^{MCNP}, C_{MCNP} = source energy MCNP neutron flux and current at the outboard shield, and ϕ^{TRD} = source energy (group 2) TRIDENT-CTR neutron flux at the outboard shield. The ONEDANT normalization was slightly different; i.e.,

$$NF = \frac{K}{C_{MCNP}} \frac{S_V^{MCNP}}{S_V^{ODN}} , \qquad (3)$$

where the terms are the same except that the last ratio, S_V^{MCNP} and S_V^{ODN}, are the volumetric source strengths in the two calculations. If the exact same normalization procedure were used for ONEDANT as was used for the TRIDENT-CTR calculations, the ONEDANT normalization factor would be approximately 10% higher.

The Monte Carlo calculations also provide some results that are of general interest and also aid in explaining the discrete-ordinates results which will be presented in the next section. Figures 8 and 9 show the angular distribution of neutrons incident on the outboard and inboard shields, respectively. The angle theta referred to in these figures is measured from the normal to the shield surface, i.e., in a positive radial direction for the outboard shield and negative radial direction for the inboard shield. From these figures the following observations can be made: (a) for each configuration the outboard and inboard angular distributions are not the same and (b) at both the outboard and inboard shields the two-dimensional spatially dependent source case yields the most sharply peaked incident angular distribution and the one-dimensional spatially uniform source case yields the least peaked angular distribution. Additional information of general interest is provided in Table III wherein for each of the three configurations the current, flux, and average angle of incident on both shields are tabulated for source-energy neutrons. This data supports the observations from Figs. 8 and 9. The figures and the table indicated that the flux to current ratio is largest for the one-dimensional spatially uniform case and smallest for the two-dimensional spatially dependent source case. Thus, even if the source-energy fluxes incident on the inboard shield were the same, the corresponding source-energy current for the one-dimensional spatially uniform source would be the smallest. Also. the source-energy flux deep within the shield and magnet would also be the smallest because the incident current was smallest and it was less peaked into the shield, i.e., the incident angular distribution was more isotropic.

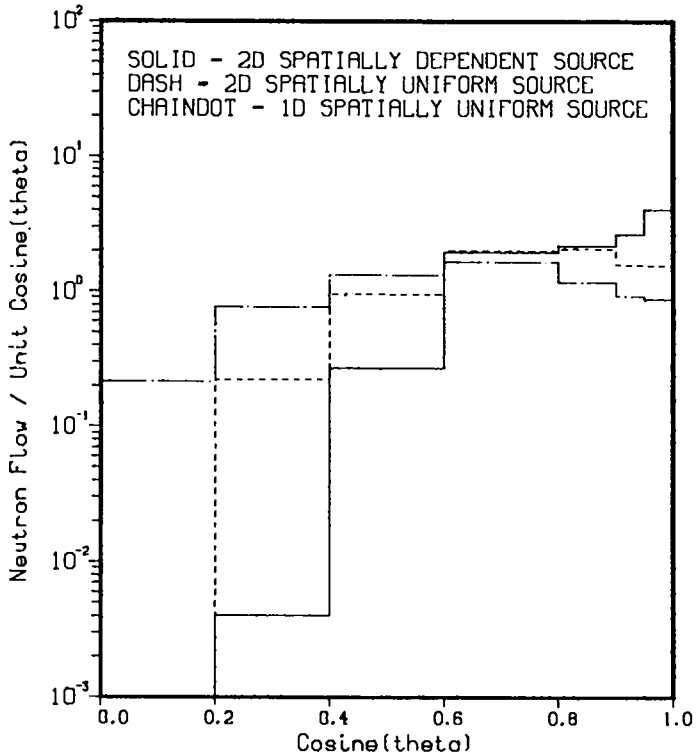

Fig. 8. Comparison of neutron angular distribution at the outboard shield/plasma chamber interface.

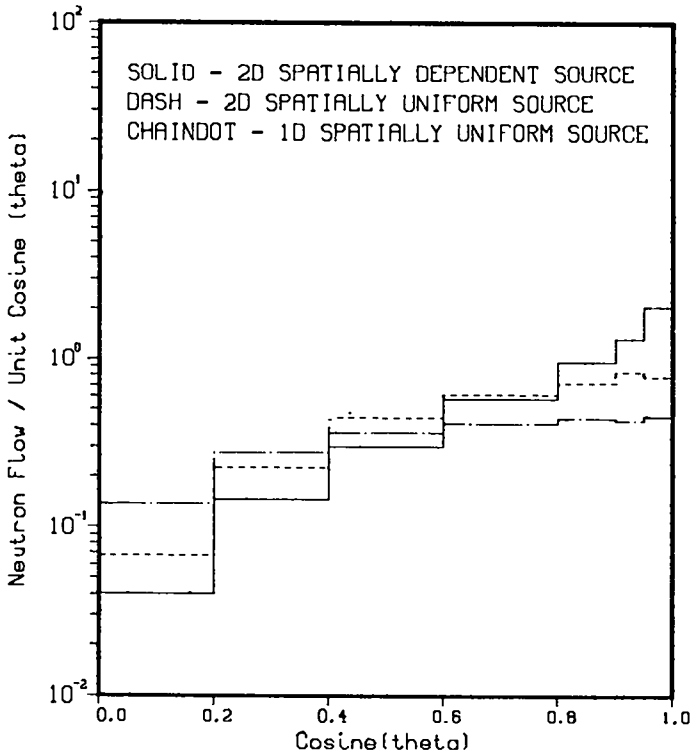

Fig. 9. Comparison of neutron angular distribution at the inboard shield/plasma chamber interface.

TABLE III

MCNP NEUTRON PARAMETERS AT THE INBOARD AND OUTBOARD SHIELD/PLASMA CHAMBER INTERFACE

	ONEDANT	TRIDENT-CTR	
		Uniform Source	(r,z) Dependent Source
Outboard Shield[a]			
Current ($cm^{-2}s^{-1}$)	1.90-6 (0.0011)[b]	2.96-7 (0.0074)	3.55-7 (0.0096)
Flux ($cm^{-2}s^{-1}$)	4.15-6 (0.0026)	4.40-7 (0.0078)	4.48-7 (0.0098)
$\langle\theta\rangle$[c] (deg)	62.7	47.7	37.7
Flux/Current	2.18	1.49	1.26
Inboard Shield[d]			
Current ($cm^{-2}s^{-1}$)	1.18-6 (0.0035)	2.38-7 (0.0115)	3.19-7 (0.0141)
Flux ($cm^{-2}s^{-1}$)	3.06-6 (0.0060)	4.53-7 (0.0163)	5.10-7 (0.0205)
$\langle\theta\rangle$ (deg)	67.3	58.3	51.3
Flux/Current	2.59	1.90	1.60

[a] At r = 6.31 m.

[b] Fractional error at the 68% confidence level.

[c] Average polar angle of incidence measured from the inward normal to the shield surface.

[d] At r = 3.31 m.

One important conclusion to be drawn is that the relationship between the flux and current varies from the outboard to the inboard shield and also that the relationship is dependent on the problem geometry and the source representation. Therefore, accurate normalization of the calculation should be based on calculations which correctly model the geometry and the source. Also, it should be clear that simply normalizing a less rigorous calculation at the inboard shield will not necessarily guarantee correctly normalized results throughout the inboard shield and TF coil magnet because it is the neutron current magnitude and angular distribution that determines the neutron fluxes deep within the shield and in the magnet.

IV. RESULTS AND DISCUSSION

This section contains the results of the two TRIDENT-CTR calculations in the form of contour and one-dimensional plots of the neutron flux and total (neutron plus gamma-ray) heating. In addition, there are intercomparisons between the two TRIDENT-CTR calculational results as well as comparison with the ONEDANT results. Finally, we compare the calculated results with the FED conceptual design criteria for the inboard TF coil magnet. All results presented in this section have been normalized to a wall loading of 0.4 MW/m^2 at the outboard-shield first wall. The reader's understanding of the plots presented will be enhanced through referral back to the geometric model as shown in Figs. 1 and 2.

In the TRIDENT-CTR calculations, no special attempt was made to handle any radiation streaming in the void gaps between the inboard shield and the TF coil magnet, i.e., no special quadrature set etc. was used. There is a potential for streaming particularly in the 0.28 m void between the magnet and the dewar. It is recognized that streaming may not be correctly calculated as discrete-ordinates codes in general have difficulty with streaming in long, narrow void channels. However, given the physics of the configurations considered in this effort, it is not expected either that streaming will be overly significant or that it impacts heavily on the conclusions presented. This discussion is pursued further as the individual contour plots are discussed.

Results of the TRIDENT-CTR spatially dependent source calculations are presented in Figs. 10 through 17. A contour plot of the total neutron flux is provided in Fig. 10. The saw-toothed nature of the contours in the upper right of this figure results from overlaying a rectangular plotting mesh onto the triangular mesh within the slanted portion of the geometry. Figure 11 presents the same total neutron flux contours but for only the inboard portion of the configuration. At locations between approximately 2.0 and 2.5 m from the torus centerline, i.e., at the void gap between the magnet and the dewar, there is some evidence of streaming. On the basis of the physics of the problem, there is little reason to expect significant streaming over most of the axial extent of the void included in this problem. Examination of the flux profiles in the inboard shield indicate that a more-or-less constant flux is entering the void gap. At large distances ($\geq$2.0 m) above the torus midplane, evidence of streaming is seen, and at higher elevations it is logical for the streaming to become more predominant in the gap

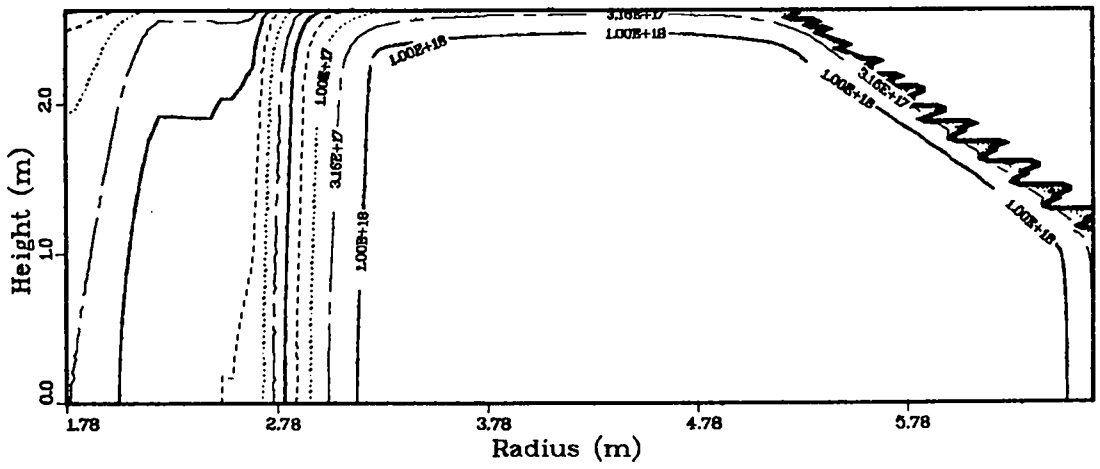

Fig. 10. TRIDENT-CTR total neutron flux ($m^{-2}s^{-1}$) for the spatially dependent source case. See Fig. 1 for the geometric model.

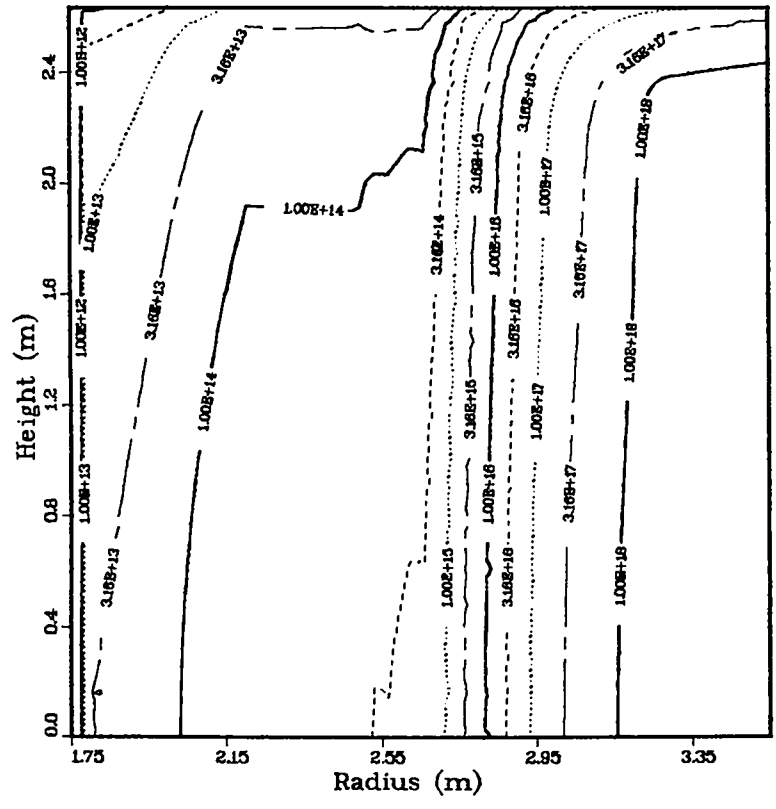

Fig. 11. TRIDENT-CTR total neutron flux ($m^{-2}s^{-1}$) for the spatially dependent source case. See Fig. 1 for the geometric model.

and in the materials immediately adjacent. Figures 12 and 13 provide contour plots of the total heating for both the full and inboard portions of the problem, respectively.

One-dimensional plots of the total neutron flux and the total heating are presented in Figs. 14 through 17. These plots provide a more detailed display of the flux and heating rate variation through the inboard portion of the problem. Figures 14 and 15 are radial profiles at various axial heights of the flux and heating, respectively. Similarly, Figs. 16 and 17 are axial profiles of the flux heating, respectively, at various radial locations. The reader is directed to Figs. 1 and 2 for a better understanding of the locations of these one-dimensional plots.

Figures 18 through 25 present similar contour and one-dimensional plots of the total neutron flux and total heating for the TRIDENT-CTR calculation using the spatially uniform source. In particular, Figs. 18 and 19 are neutron flux contour plots for the full configuration and the inboard shield/magnet, respectively, and Figs. 20 and 21 are the corresponding contour plots of the heating. Similarly, Figs. 22 and 23 and Figs. 24 and 25 are one-dimensional plots of flux and heating as a function of radius at various axial locations and as a function of axial height at various radial location, respectively.

The corresponding plots in each set of figures, i.e., Figs. 10 through 17 and Figs. 18 through 25, have curves which are similar in shape and magnitude. Therefore, a careful examination of the plots is necessary to identify the differences.

Prior to looking at specific comparisons, it can be seen that for the spatially dependent source case there is a little more evidence of streaming in the void region between the magnet and the inboard shield and also that the contours in the inboard shield have more curvature with height toward the plasma as compared to the results from the spatially uniform source calculations. These differences as well as those yet to be presented are traceable to the difference in the source, which was the only difference between the two calculations. In particular, in the spatially dependent source case the source is more highly concentrated in the center of the plasma chamber, therefore yielding a more highly peaked source-energy current into the shields at the equatorial midplane. This results in higher neutron fluxes deep within the shield and into the magnet as the 14-MeV neutrons

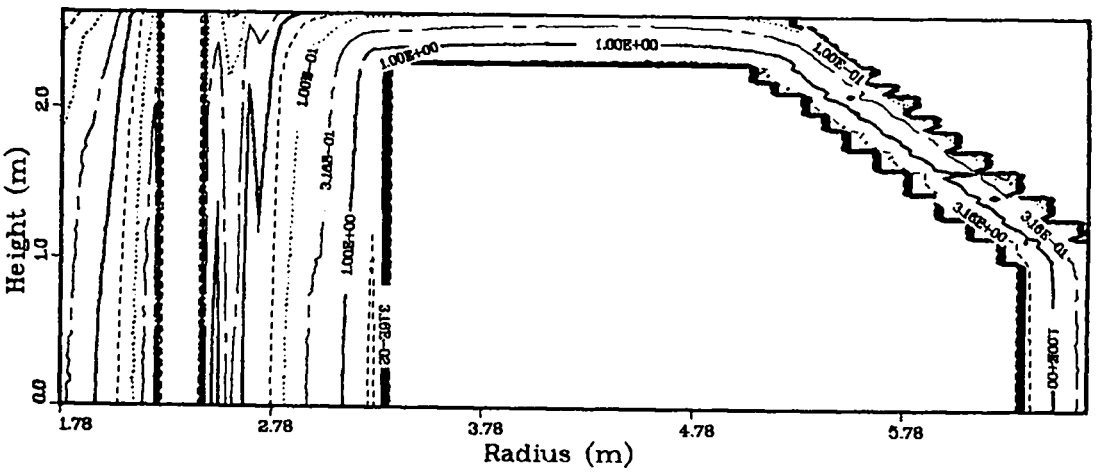

Fig. 12. TRIDENT-CTR total nuclear heating (MW/m^3) for the spatially dependent source case. See Fig. 1 for the geometric model.

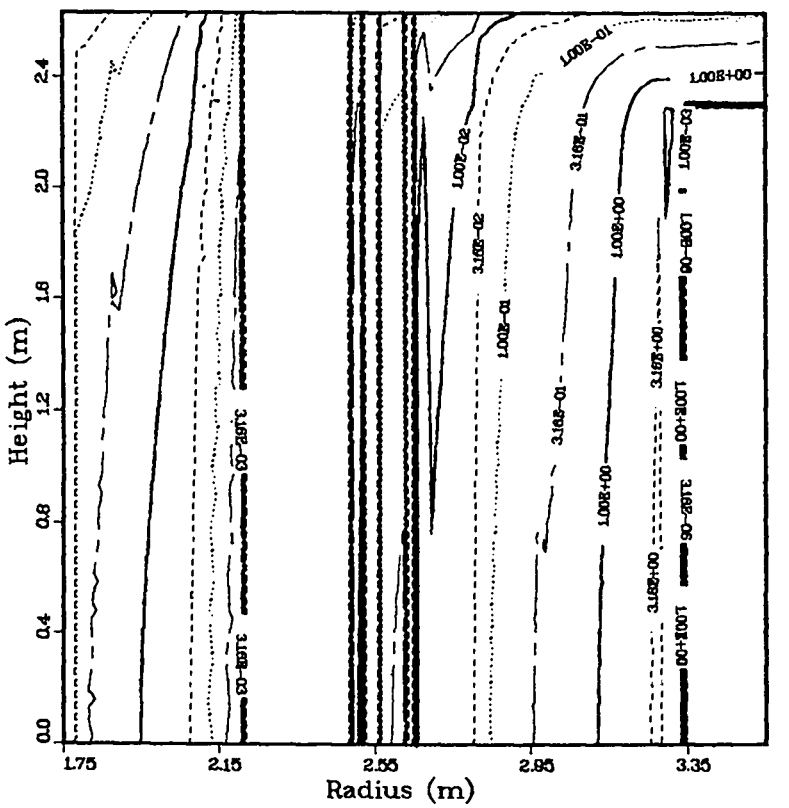

Fig. 13. TRIDENT-CTR total nuclear heating (MW/m^3) for the spatially dependent source case. See Fig. 1 for the geometric model.

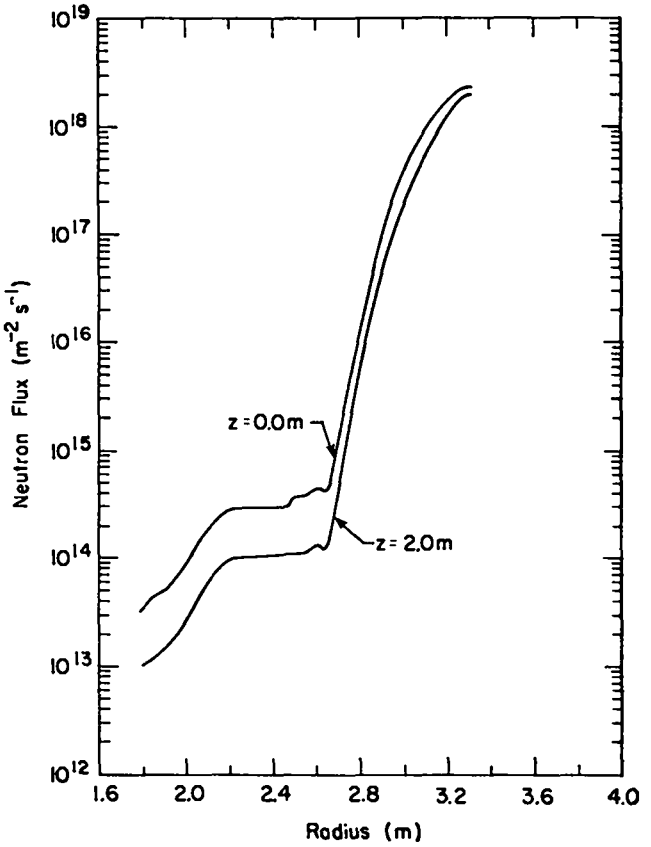

Fig. 14. TRIDENT-CTR neutron flux versus radial distance from the torus centerline for the spatially dependent source case.

are the source (through down scattering) for all other neutron groups. In addition, because the source is more concentrated, as opposed to the uniform source case, the magnitude of the flux entering the void regions between the inboard shield and the magnet has more variation and thus the degree of neutron streaming is somewhat more pronounced.

The ratio of total neutron fluxes, i.e., the spatially dependent source case flux to the spatially uniform source case flux, versus radius is shown in Fig. 26 at two axial locations, at z = 0.0 and z = 2.0 m above the equatorial midplane. These two curves illustrate much of what was alluded to previously. In particular, at z = 0.0 m the flux ratio in the shield and magnet is governed by the highly

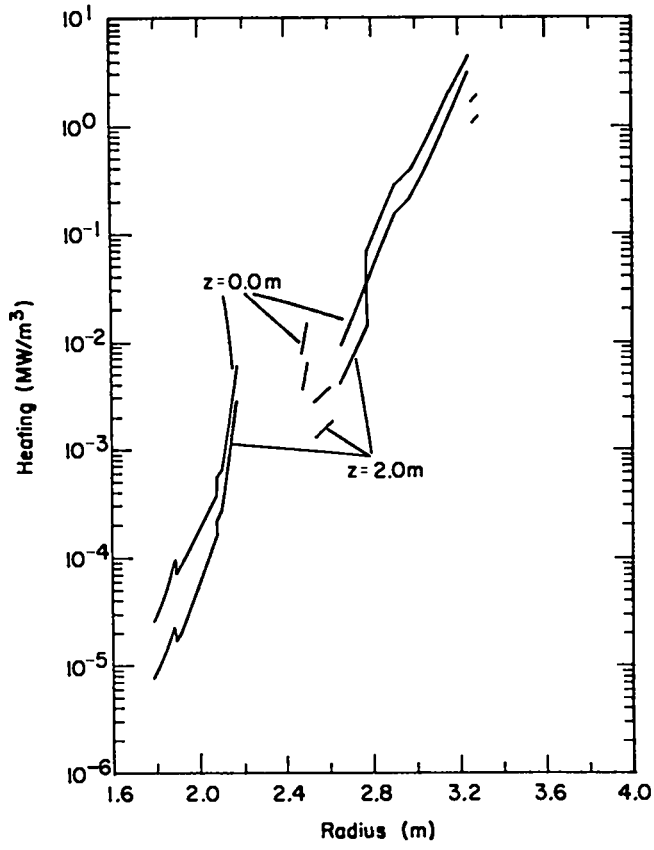

Fig. 15. TRIDENT-CTR total nuclear heating versus radial distance from the torus centerline for the spatially dependent source case.

peaked 14-MeV neutron angular distribution incident on the inboard shield of the spatially dependent source case and the mediating effect of the void regions. At z = 2.0 m, the ratio appears to be a reflection of that at z = 0.0 m, with the spatially uniform source case flux dominating.

Figure 27 presents a comparison of the neutron flux spectrum at the first meshpoint in the TF coil magnet, i.e., r = 2.0925 m. It is seen that the two spectra are nearly identical in shape and that the spatially uniform case results in slightly lower values. This result is consistent with the previously presented data.

A pointwise comparison of data from the two TRIDENT-CTR calculations and the ONEDANT calculation is presented in Table IV. The outboard-shield wall loadings are identical as all three calculations were normalized to 0.4 MW/m^2 at this location. The ONEDANT results are clearly the largest at the carbon armor and

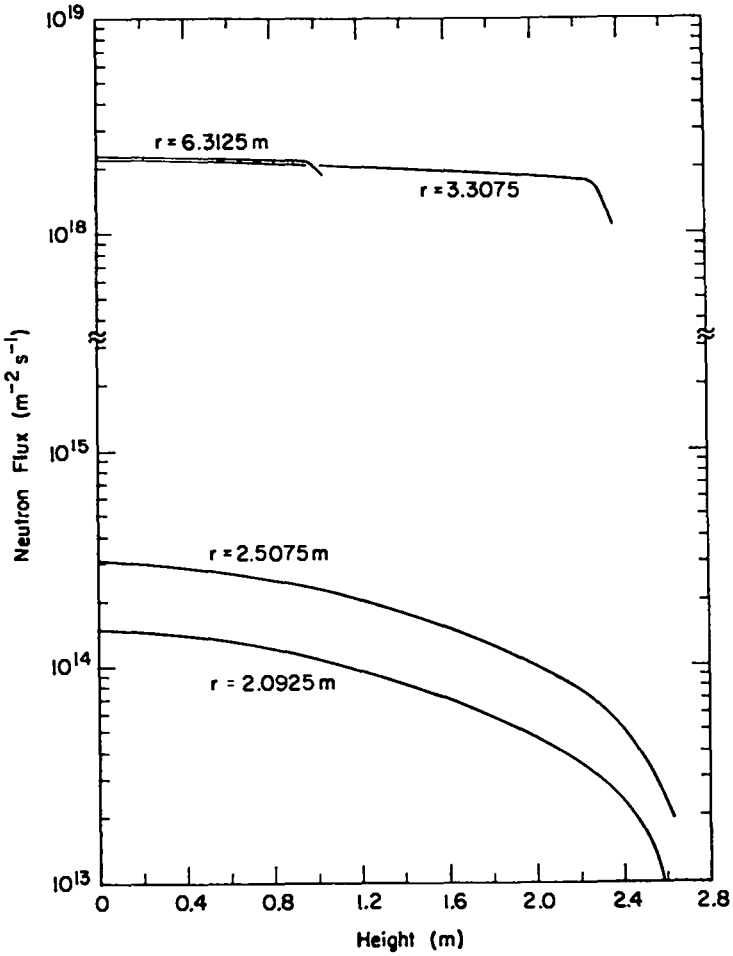

Fig. 16. TRIDENT-CTR total neutron flux versus axial height above the equatorial midplane of the torus for the spatially dependent source case.

the lowest at locations inboard of the inboard shield, i.e., $r < 2.66$ m, whereas the TRIDENT-CTR results for the spatially dependent source case are the lowest and the highest at these same two locations, respectively. These numerical results are consistent with the effects of geometry and source representation discussed earlier in this section and the incident angular distributions for each of the three cases as presented and discussed in Sec. III.

Comparison of the results presented in Table IV and the TRIDENT-CTR spatially dependent source case contour and one-dimensional plots, Figs. 10 to 17, to the

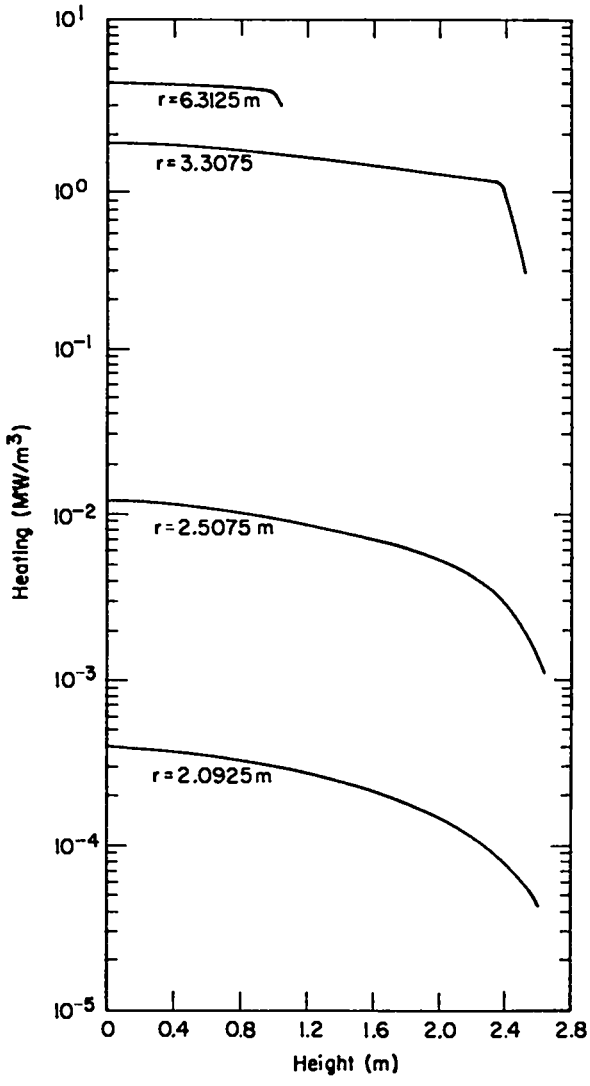

Fig. 17. TRIDENT-CTR total nuclear heating versus height above the equatorial midplane of the torus for the spatially dependent source case.

FED design criteria[8] provides an evaluation of the inboard shield with respect to the TF coil design limits. In particular, the TF coil design criteria for normal 8-telsa operation are: G10CR insulation lifetime dose, 10^7 Gray; damage to the TF coil copper stabilizer for 25% resistivity increase, 3.0×10^{-4} dpa (8.6×10^{12} dpa/s); and nuclear heating in the inboard TF coil magnet, 5 mW/cm^3 maximum. The copper dpa and G10CR dose values are based on a reactor life of 3.5×10^7 s. The nuclear heating criteria of 5 mW/cm^3 is for the initial

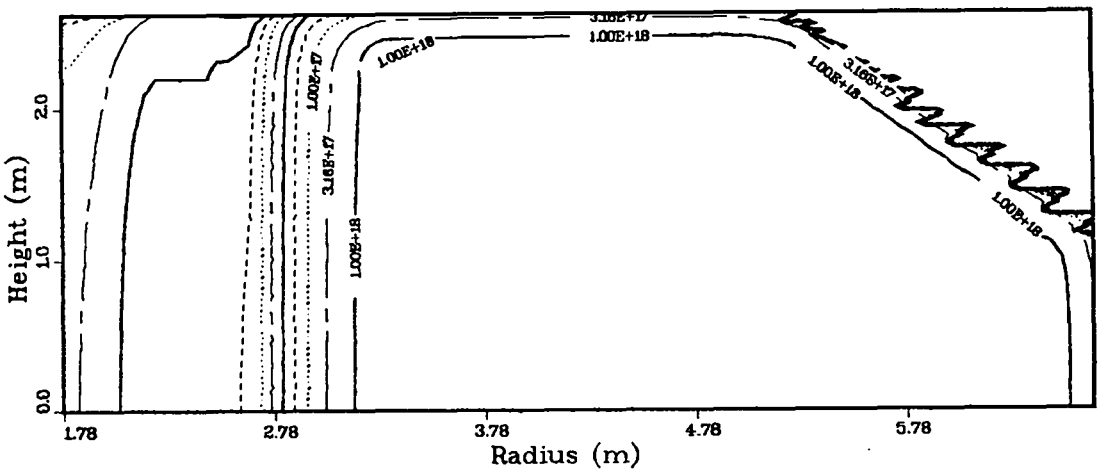

Fig. 18. TRIDENT-CTR total neutron flux ($m^{-2}s^{-1}$) for the spatially uniform source case. See Fig. 1 for the geometric model.

heating in the TF coil magnet structure, whereas the values in Table IV are the initial values in the TF coil itself. Calculated values at the first mesh point in the TF coil magnet structure are slightly above the design criteria. However, an integral calculation of the entire inboard TF coil magnet (coil plus support structure) should be made and compared to total refrigeration requirements before judging the adequacy of the inboard shield on the basis of the nuclear heating criteria.

V. CONCLUSIONS

In three different discrete-ordinates calculations, two different geometric models and three different source representations for the FED have been considered. Results of these calculations have illustrated the potential for underpredicting nuclear responses at the inboard TF coil using a one-dimensional calculation. Furthermore, it was demonstrated that a two-dimensional calculation using a spatially uniform source yields results in the TF coil which are higher than those from a one-dimensional calculation but slightly less than those obtained from a two-dimensional calculation using a spatially dependent source. The results at the inboard TF coil have indicated the adequacy of the conceptual

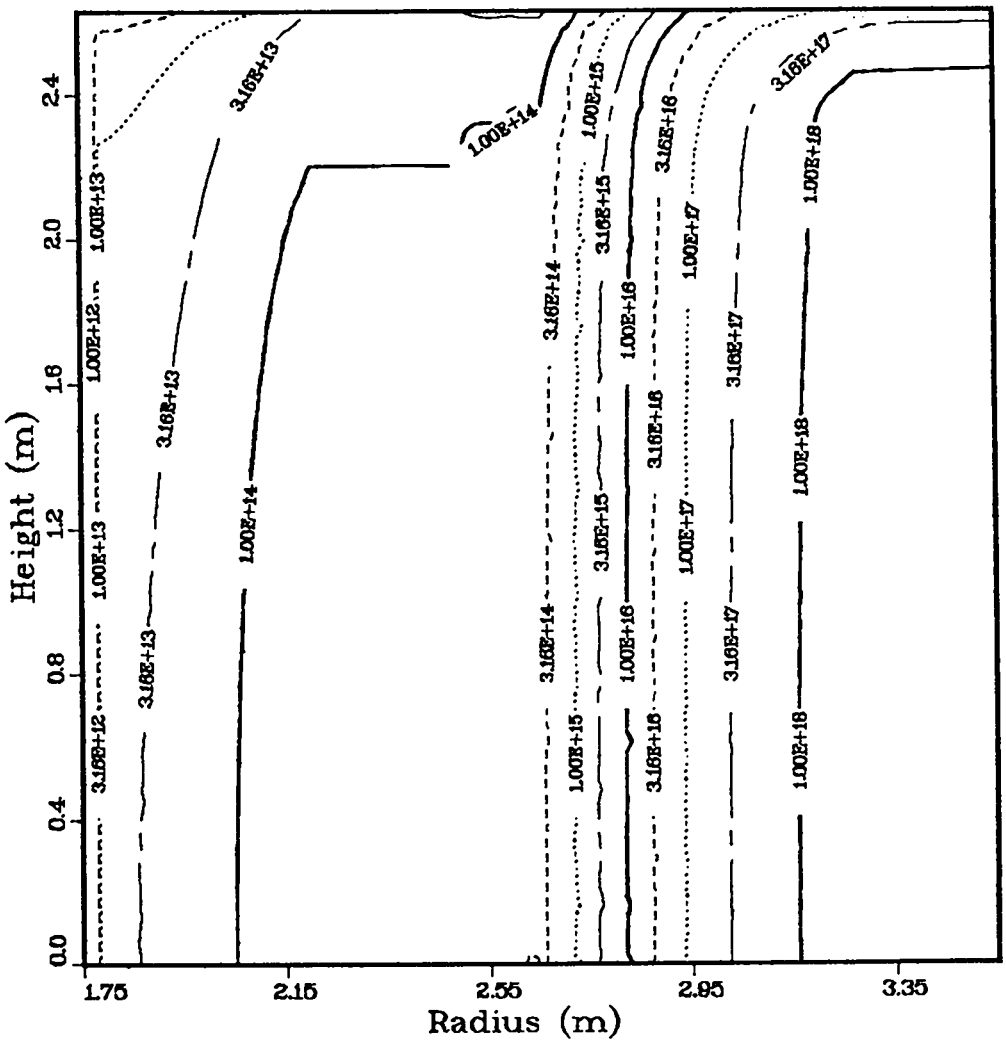

Fig. 19. TRIDENT-CTR total neutron flux ($m^{-2}s^{-1}$) for the spatially uniform source case. See Fig. 1 for the geometric model.

inboard shield to limit copper dpa and dose to the G10CR insulation to less than the design criteria. Nuclear heating results are slightly above the design criteria, however, an integral calculation of the total heating in the inboard TF coil and support structure should be made to determine total refrigeration requirements prior to judging the inboard shield inadequate on the basis of nuclear heating criteria. Comparison of the incident neutron angular distributions on the inboard and outboard shield has illustrated the influence of geometry and source modeling and, furthermore, the difficulty of normalizing one-dimensional calculations to obtain two-dimensional calculational accuracy throughout the inboard shield and magnet.

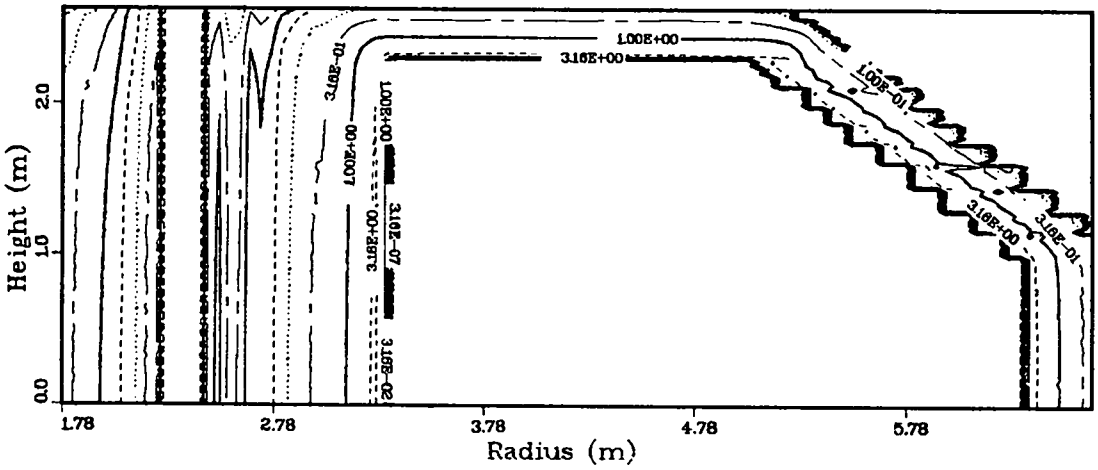

Fig. 20. TRIDENT-CTR total nuclear heating (MW/m^3) for the spatially uniform source case. See Fig. 1 for the geometric model.

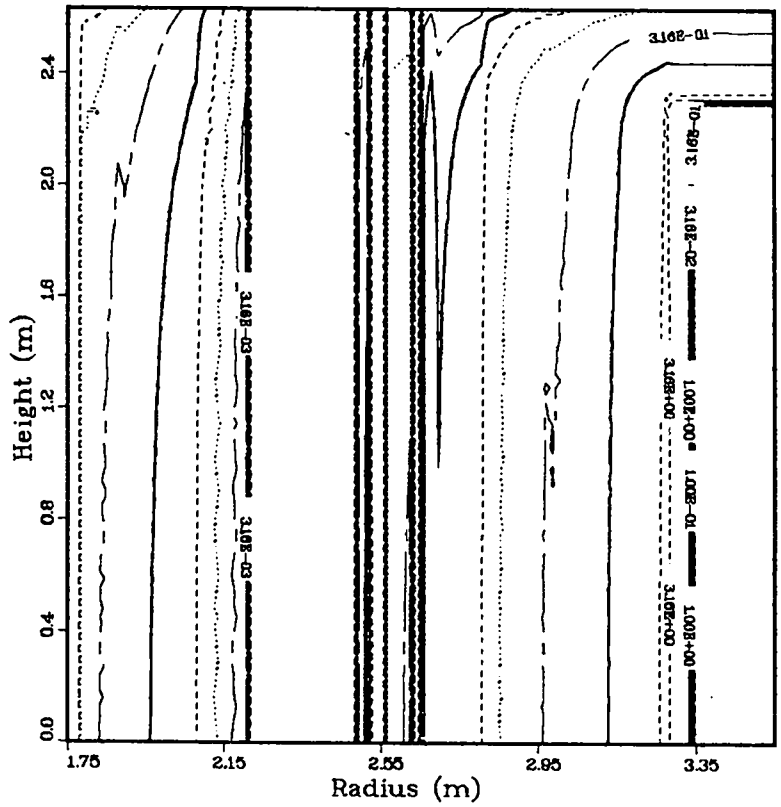

Fig. 21. TRIDENT-CTR total nuclear heating (MW/m^3) for the spatially uniform source case. See Fig. 1 for the geometric model.

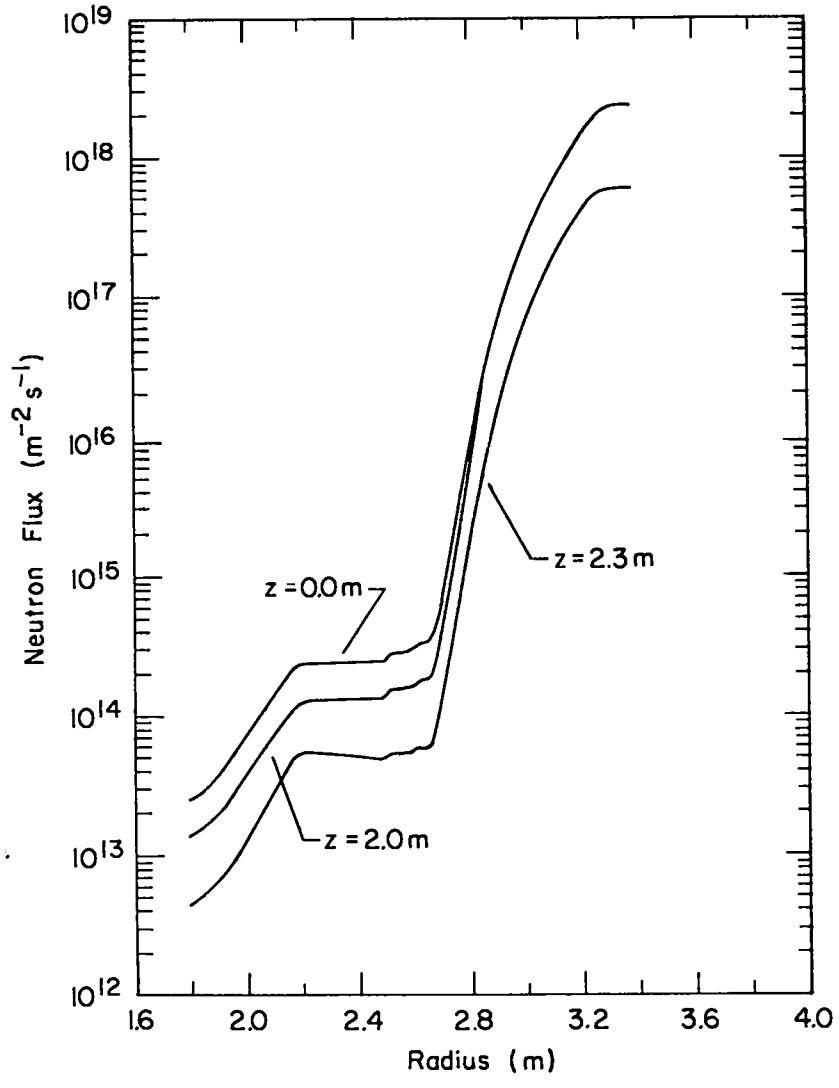

Fig. 22. TRIDENT-CTR total neutron flux versus radial distance from torus centerline for the spatially uniform case.

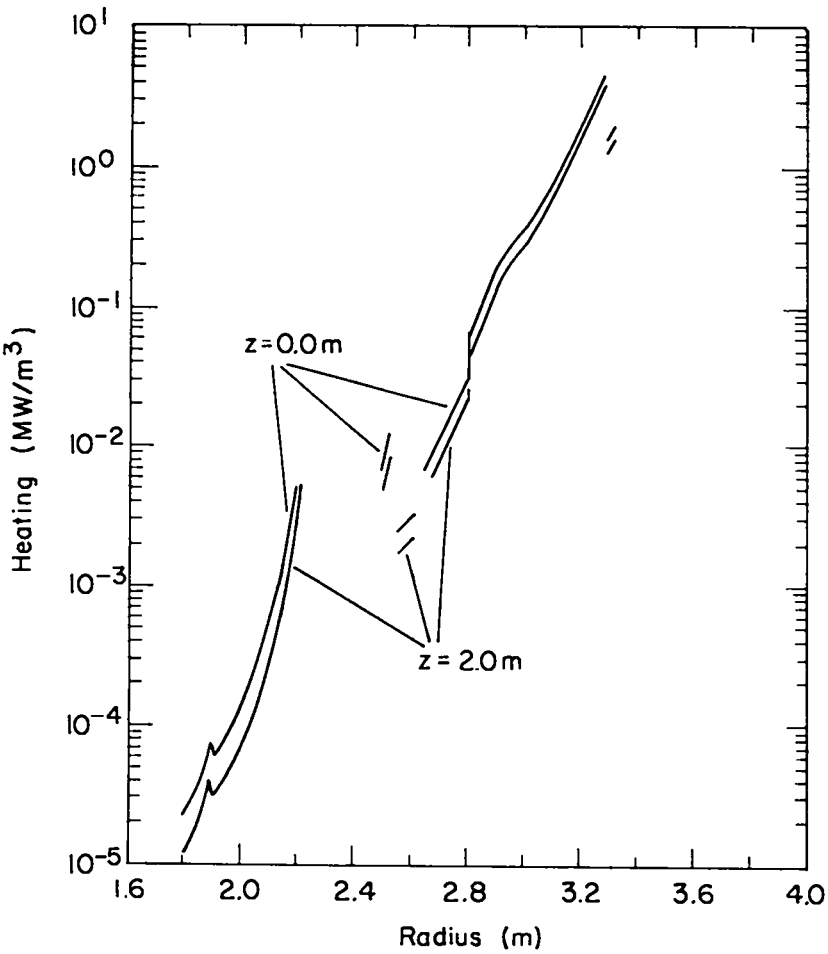

Fig. 23. TRIDENT-CTR total nuclear heating versus radial distance from the torus centerline for the spatially uniform source case.

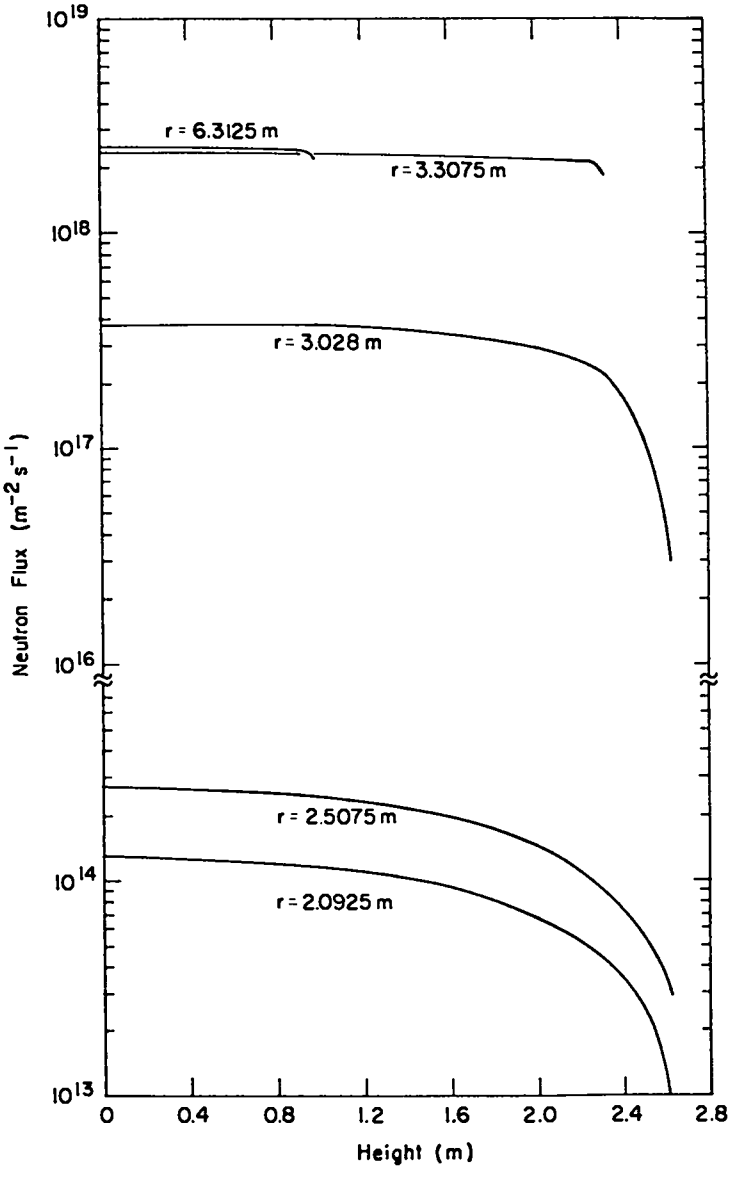

Fig. 24. TRIDENT-CTR total neutron flux versus axial height above the equatorial midplane of the torus for the spatially uniform source case.

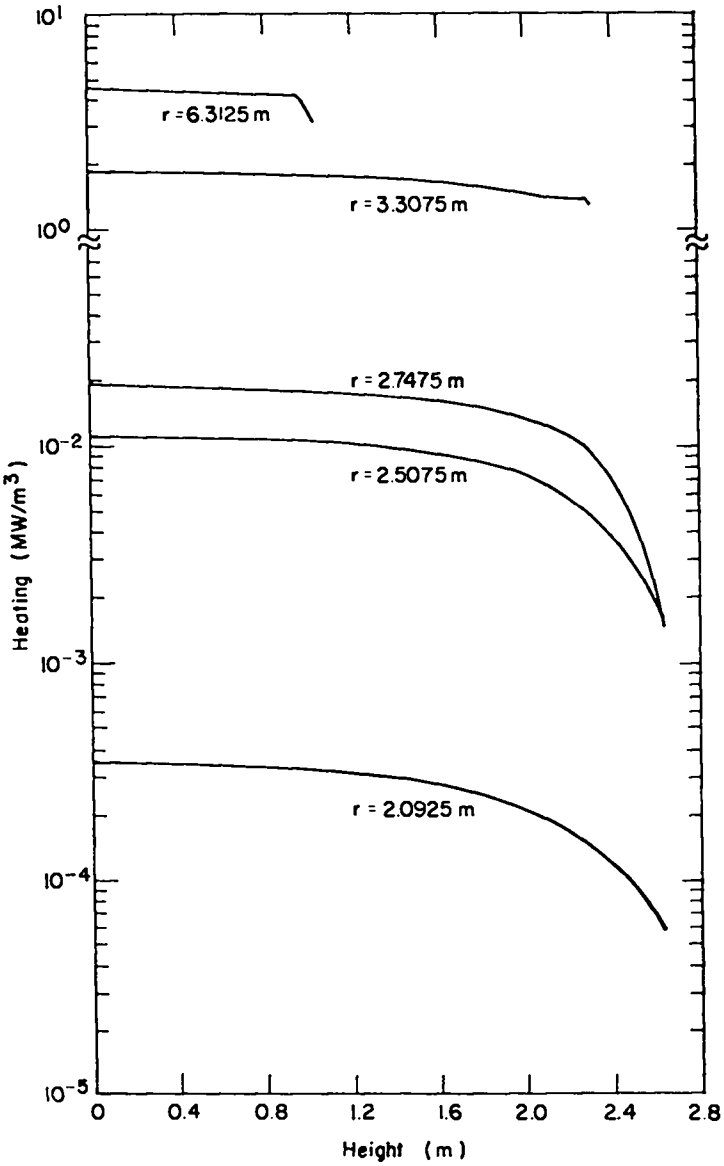

Fig. 25. TRIDENT-CTR total nuclear heating versus axial height above the equatorial midplane of the torus for the spatially uniform source case.

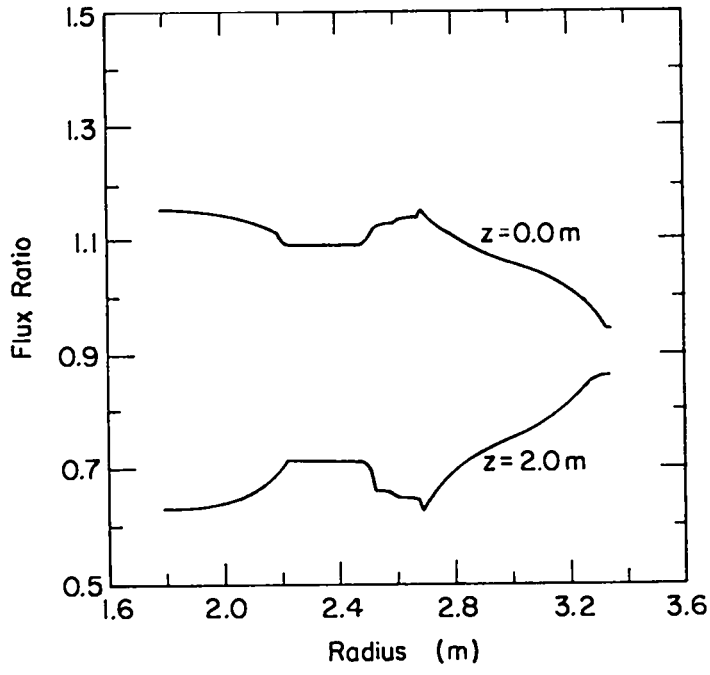

Fig. 26. Ratio of TRIDENT-CTR total neutron fluxes, spatially dependent source case to the spatially uniform source case, versus radial distance from the torus centerline.

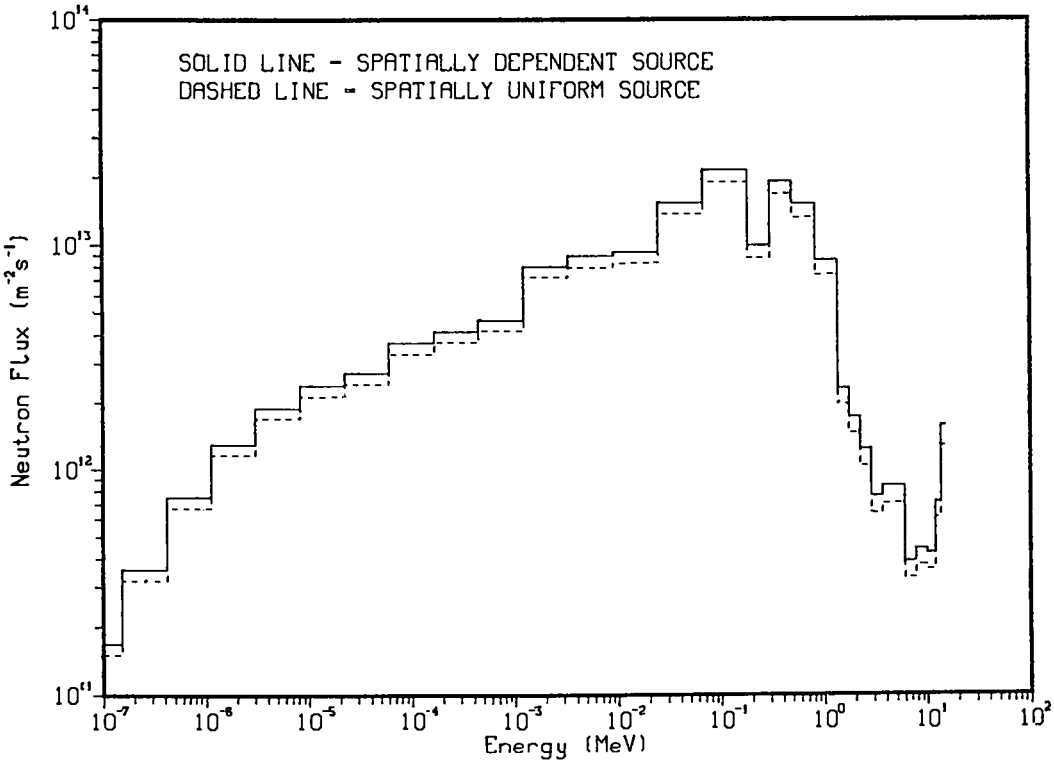

Fig. 27. TRIDENT-CTR neutron flux spectra in the TF coil, r = 2.0925 m, for the spatially dependent and spatially uniform source case.

TABLE IV

COMPARISON OF ONEDANT AND TRIDENT-CTR RESULTS[a]

Location[b]	Radius (m)	Quantity (units)	ONEDANT	TRIDENT-CTR	
				Uniform Source	Distributed Source
Outboard Shield	6.31	Wall Loading (MW/m^2)	0.40	0.40	0.40
Inboard	3.31	Wall Loading (MW/m^2)	0.25	0.32	0.35
Carbon Armor	3.3075	14-MeV Flux[c] ($m^{-2}s^{-1}$)	2.8 + 17[d]	2.6 + 17	2.4 + 17
	3.3075	Total Flux[e] ($m^{-2}s^{-1}$)	2.6 + 18	2.4 + 18	2.2 + 18
	3.3075	Total Heating[f] (MW/m^3)	2.2	1.9	1.8
Inboard-Shield Can	2.6575	14-MeV Flux ($m^{-2}s^{-1}$)	8.0 + 12	1.2 + 13	1.5 + 13
	2.6575	Total Flux ($m^{-2}s^{-1}$)	3.0 + 14	3.5 + 14	3.9 + 14
Dewar	2.5075	14-MeV Flux ($m^{-2}s^{-1}$)	6.3 + 12	9.0 + 12	1.1 + 13
	2.5075	Total Flux ($m^{-2}s^{-1}$)	2.3 + 14	2.7 + 14	3.0 + 14
	2.5075	Total Heating (MW/m^3)	1.0 - 2	1.1 - 2	1.2 2
TF Coil	2.0925	14-MeV Flux ($m^{-2}s^{-1}$)	8.9 + 11	1.3 + 12	1.6 + 12
	2.0925	Total Flux ($m^{-2}s^{-1}$)	1.0 + 14	1.3 + 14	1.5 + 14
	2.0925	Total Heating (MW/m^3)	3.1 - 4	3.5 - 4	3.8 - 4
	2.0925	Copper Damage (dpa/s)	3.8 - 12	4.9 - 12	5.7 - 12
	2.0925	G10CR Dose (Gray/r.l.)[g]	4.1 + 6	5.0 + 6	5.6 + 6

[a] Results at the equatorial midplane of the torus.
[b] Refer to Fig. 1 for geometric locations.
[c] Neutron energy group 2 flux, 13.5 < E < 15.0 MeV.
[d] 2.8 + 17 = 2.8×10^{17}.
[e] Total neutron flux.
[f] Neutron plus gamma-ray heating.
[g] Gray/r.l. = Gray/reactor life = Gray/3.5×10^7 s.

REFERENCES

1. R. D. O'Dell, F. W. Brinkley, Jr., and D. R. Marr, "User's Manual for ONEDANT: A Code Package for One-Dimensional, Diffusion-Accelerated, Neutral Particle Transport," Los Alamos National Laboratory report LA-9184-M (February 1982).

2. T. J. Seed, "TRIDENT-CTR User's Manual," Los Alamos Scientific Laboratory report LA-7835-M (May 1979).

3. Los Alamos Group X-6, "MCNP-A General Monte Carlo code for Neutron and Photon Transport," Los Alamos Scientific Laboratory report LA-7396-M, Revised (November 1979).

4. C. I. Baxman and P. G. Young, "Applied Nuclear Data Research and Development January 1 - March 31, 1977," Los Alamos Scientific Laboratory report LA-6893-PR (July 1977).

5. R. E. MacFarlane and R. J. Barrett to Distribution, "TRANSX," Los Alamos Scientific Laboratory document T-2-L-2923, August 24, 1978.

6. G. I. Bell, G. E. Hansen, and H. A. Sandmeier, "Multitable Treatments of Anisotropic Scattering in S_N Multigroup Transport Calculations," Nucl. Sci. Eng. 28, 376 (1967).

7. B. G. Carlson, "Tables of Symmetric Equal Weight Quadrature EQ_N Over the Unit Sphere," Los Alamos Scientific Laboratory report LA-4734 (July 1971).

8. B. A. Engholm, "Status of FED Shielding Analysis and Design," General Atomic Company report GA-A16499 (September 1981).

Printed in the United States of America
Available from
National Technical Information Service
US Department of Commerce
5285 Port Royal Road
Springfield, VA 22161

Microfiche (A01)

Page Range	NTIS Price Code	Page Range	NTIS Price Code	Page Range	NTIS Price Code	Page Range	NTIS Price Code
001-025	A02	151-175	A08	301-325	A14	451-475	A20
026-050	A03	176-200	A09	326-350	A15	476-500	A21
051-075	A04	201-225	A10	351-375	A16	501-525	A22
076-100	A05	226-250	A11	376-400	A17	526-550	A23
101-125	A06	251-275	A12	401-425	A18	551-575	A24
126-150	A07	276-300	A13	426-450	A19	576-600	A25
						601-up*	A99

*Contact NTIS for a price quote.

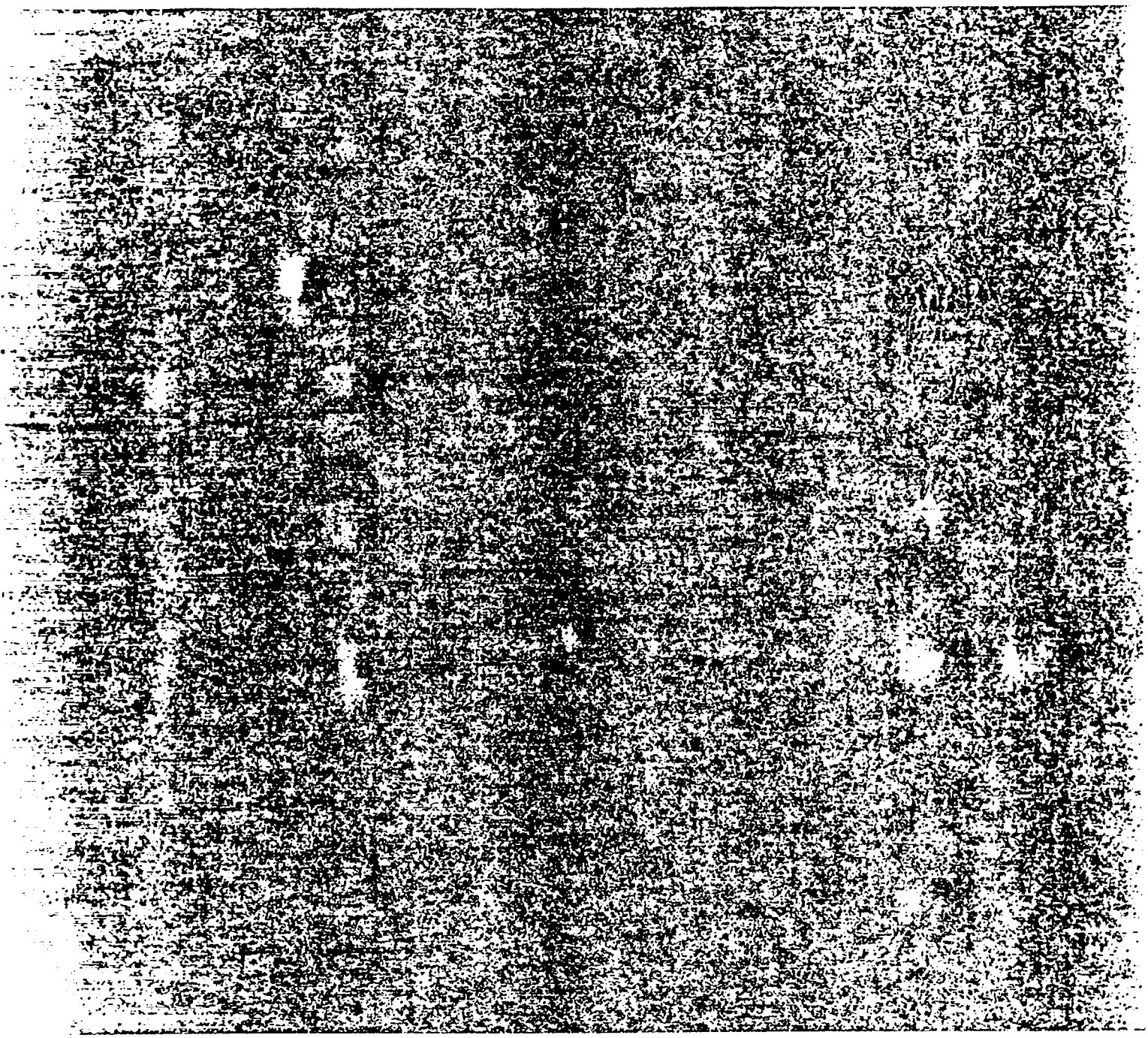

Los Alamos